

# Ring-shaped spatial pattern of exciton luminescence formed due to the hot carrier transport in locally photoexcited electron-hole bilayer

A. V. Paraskevov<sup>1,2</sup>

<sup>1</sup>*National Research Center "Kurchatov Institute", Kurchatov Sq. 1, Moscow 123182, Russia*

<sup>2</sup>*Department of Physics, Loughborough University, Loughborough LE11 3TU, United Kingdom*

A consistent explanation of the formation of a ring-shaped pattern of exciton luminescence in GaAs/AlGaAs double quantum wells is suggested. The pattern consists of two concentric rings around the laser excitation spot. It is shown that the luminescence rings appear due to the in-layer transport of hot charge carriers at high photoexcitation intensity. Interestingly, one of two causes of this transport might involve self-organized criticality (SOC) that would be the first case of the SOC observation in semiconductor physics. We test this cause in many-body numerical model by performing extensive molecular-dynamics simulations. The results show good agreement with experiments. Moreover, the simulations have enabled us to identify the particular kinetic processes underlying the formation of each of these two luminescence rings.

PACS numbers: 71.35.-y, 78.60.-b, 78.67.De

## INTRODUCTION

Non-equilibrium collective effects in the exciton and exciton-polariton systems in semiconductor heterostructures are a subject of intensive studies [1–26]. A particular attention has been focused on the beautiful phenomenon discovered experimentally in the system of interwell excitons in GaAs/AlGaAs double quantum wells (QWs) [6]: at high enough excitation intensity a local photoexcitation of electrons (e) and holes (h) above the exciton resonance gave rise to a macroscopic ring-shaped pattern of spatial distribution of the exciton luminescence. The radius of the ring can be varied in a wide range by tuning external parameters such as excitation intensity or gate voltage. Remarkably, at sub-Kelvin lattice temperatures the stationary ring exhibits a sharp fragmentation which could be the signature of a non-equilibrium macroscopic quantum effect.

To understand the nature of the ring-shaped pattern, one should build a many-body model that captures local generation of electron-hole pairs and their spatial dynamics accompanied by the processes of formation and recombination of excitons. If the exciton lifetime is long enough, one should also consider the spatial dynamics of the excitons.

The first theoretical explanation which met these requirements was based [13, 14, 16, 17] on the diffusive transport model (DTM) applied to the locally photo-generated holes and equilibrium electrons which initially were uniformly distributed in the quantum-well plane. The overlapping region for the hole and electron spatial distributions apparently gave rise to the ring of exciton luminescence.

However, this explanation has a lot of evident shortcomings [27]. For example, if one adds the same number of photogenerated electrons in the model (in principle, they must be added to keep electroneutrality), then the ring of exciton luminescence can disappear due to the

exciton formation term, which is simply proportional to the product of the electron and hole densities. (If these densities decrease monotonically from the excitation spot center, the luminescence intensity would apparently follow them.) More specific shortcomings can be found in Appendix A. Sadly, the authors of Ref. [13], being aware of these, persistently apply their theory to explain new experimental data [24]. As we will show here, the underlying physics is much more rich.

In this paper a consistent explanation of the ring-shaped pattern formation is given. The main idea is that there appears an essential in-plane electric field in the excitation spot region at high enough excitation power. This field strongly affects the spatial dynamics of the photogenerated electrons and holes. (We do not consider any equilibrium carriers at all.) It is shown that there are contributions to the electric field from two quite different physical processes. Essentially, due to the one of these contributions the ring-shaped pattern formation could be understood in the paradigm of self-organized criticality (SOC) [28]. To test the contribution, we have performed extensive molecular-dynamics simulations. They have shown that only this contribution is quite enough for the detailed qualitative explanation of the ring-shaped pattern. (However, this paper does not concern the transition to the SOC regime. The parameters for the simulations have been chosen to be in this regime from the very beginning.)

This paper is organized as follows. Further in this Section we introduce some essential properties of double quantum wells and interwell exciton formation, some experimental results we focus on, and the formulation of the problem for the research. In Section 2 we suggest two qualitative explanations ("scenarios") for the ring-shaped pattern formation and make the corresponding estimates. Section 3 describes many-body dynamical model and conditions of the molecular-dynamics simulations performed to investigate the second scenario in

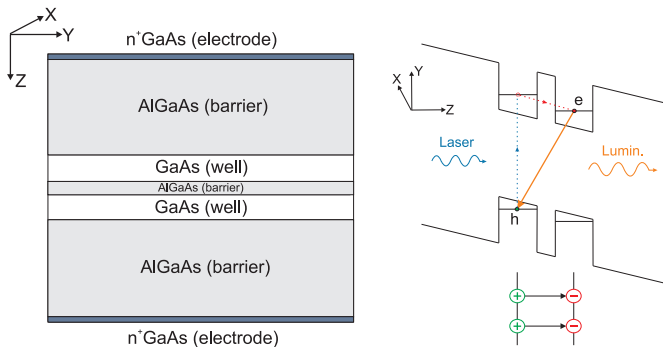


Figure 1: Left: Schematic of a double quantum well (DQW). The DQW structure is bordered by highly-doped GaAs layers that serve as external electrodes forming a plane capacitor. In experiments [6, 13, 24] widths of the layers between the electrodes are  $(200\text{ nm})(8\text{ nm})(4\text{ nm})(8\text{ nm})(200\text{ nm})$ , respectively. Right: (Top) Schematic of (i) the DQW energy profile along the "growth" axis (Z axis) when there is a voltage applied between the external electrodes (it results in a linear bias of the profile) and (ii) interwell exciton formation (arrows show the path of a photoexcited electron). (Bottom) Interwell excitons as co-directed classical dipoles.

more details. Section 4 contains the results of the simulations. Section 5 is conclusion and discussion. Finally, Section 6 consists of three Appendixes.

The structure of double QWs used in the experiments [6, 13, 24] is shown in Fig. 1(left). The electron band-gap energy  $E_{gap}$  of the "barrier" (B) layers is larger than the one of the "well" (W) layers (Fig. 1(right)) so that GaAs layers form two rectangular potential wells with the depth  $U_{QW} = (E_{gap}(B) - E_{gap}(W)) / 2 \approx 0.4\text{ eV}$ . At a moderate occupation of the wells (i.e., when the number of electrons in the GaAs conduction band is not macroscopically large; see next Section for details), a voltage applied to the external electrodes provides a constant tilt of the DQW potential profile (Fig. 1(right)). This "gate" voltage,  $V_g$ , is needed to separate electrons and holes in the different wells facilitating the formation of interwell excitons. The crossover between the interwell and intrawell exciton "ground" states takes place at  $V_g \approx 0.3\text{ V}$  [29]. (Since in the experiments [6, 13, 24]  $V_g > 0.3\text{ V}$ , the intrawell excitons are not discussed further.) The stationary laser pumping comes along Z axis and is used for the formation of a macroscopic number of photogenerated electron-hole pairs. In experiments [6, 13, 24] the typical laser power was several hundreds of  $\mu\text{W}$  and was focused in a spatial spot of few tens of  $\mu\text{m}$ . The pumping energy was well above the exciton resonances so that an electron was photoexcited to a high-energy level of the QW near the continuum. Due to the applied gate voltage, the electron can then tunnel to the corresponding QW. (The effective mass of an electron in GaAs is seven times smaller than the one of a heavy hole so the tunneling is essentially more probable for electrons than for holes.

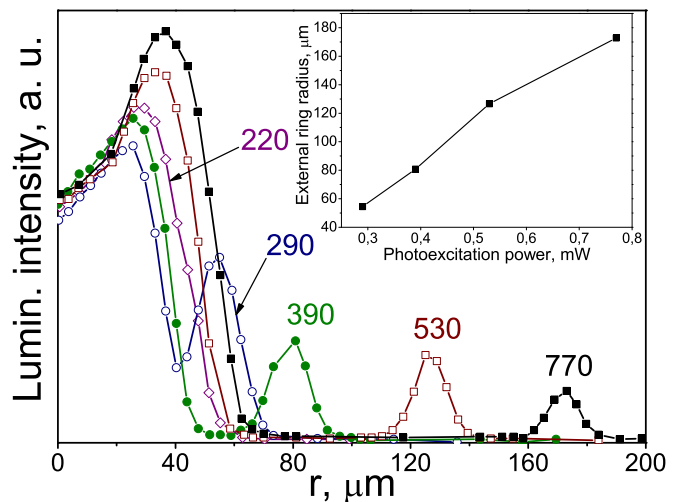


Figure 2: Experimental curves taken from Ref.[6]: luminescence intensity of interwell excitons vs distance  $r$  from the excitation spot center at different excitation powers (numbers near curves, in  $\mu\text{W}$ ). Excitation spot radius is about  $20\text{ }\mu\text{m}$ . Inset: Dependence of the external ring radius on excitation power.

Note that heavy holes have lower energy than the light ones in GaAs.) The tunneling might also be facilitated by the voltage-induced triangular profile of the barrier. Finally, after a spatiotemporal in-layer relaxation of the charge carriers, the interwell excitons are formed; they live some finite time and then annihilate giving rise to the photoluminescence (PL) pattern in the QW (X-Y) plane.

Let us now turn to the experimental results that we would like to explain (Fig. 2). At small excitation power the PL spatial profile practically follows the excitation spot (see details in [6]). When excitation power exceeds some value a thick ring of luminescence appears near the edge of the excitation spot. In Ref.[6] it was already seen at excitation power  $220\text{ }\mu\text{W}$ . Hereafter we call this ring as "internal ring". Finally, when the excitation power exceeds another critical value (Fig. 2), a thin "external" ring of luminescence appears around the excitation spot and the inner ring. Everywhere in this paper the words "ring-shaped pattern" mean these *two concentric rings*.

The formation mechanism of the ring-shaped luminescence pattern is a subject of the research described below. In particular, we pose the following questions. (i) Why does the ring-shaped pattern appear only when the laser excitation power exceeds some critical values? (ii) What are the kinetic processes which underlie the formation of the internal and external rings? (iii) Why does the external ring radius depend strongly on the static gate voltage  $V_g$  [30]? (iv) Why the luminescence of intrawell excitons (i.e., purely "two-dimensional" excitons) does not exhibit the ring-shaped pattern [6]?

## TWO SCENARIOS OF THE RING-SHAPED LUMINESCENCE PATTERN FORMATION

In general, we believe that the ring-shaped PL pattern appears due to the transport of hot uncoupled electrons and holes from the excitation spot at high enough excitation power. During the spatial spread the carriers relax in kinetic energy emitting phonons and finally can form excitons relatively far away from the excitation spot ("far away" - in comparison with the spot radius). We suppose that the hot charge carriers are formed due to (i) in-layer electric fields that occur at high pumping power in the excitation spot region and (ii) high mobilities of the charge carriers in GaAs. We suggest two particular mechanisms of the electric field occurrence; they are described in details in next subsections.

### First scenario: hot carrier transport induced by the external gate voltage

The first scenario concerns the screening of the gate voltage  $V_g$  by photogenerated carriers in the excitation spot (Fig. 3) at high excitation power.

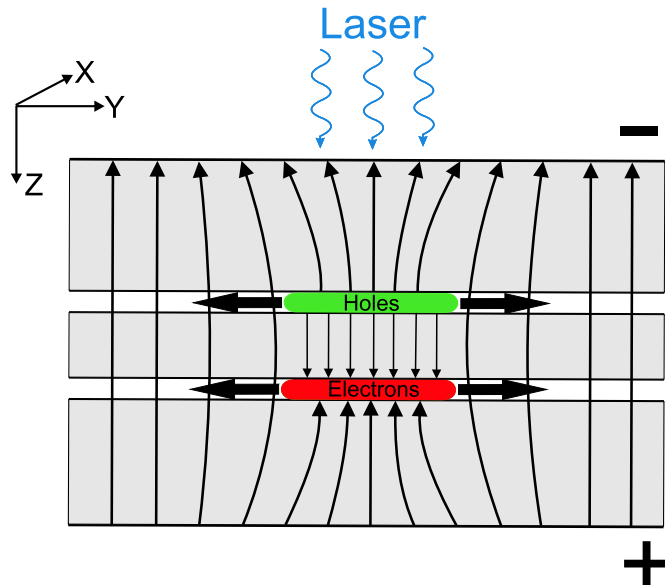


Figure 3: Schematic of the electric field distribution along the growth axis ( $Z$  axis) of DQW structure at high excitation power. In the excitation spot region (green and red ovals in the center) the static electric field induced by external gate voltage is curved due to the presence of a macroscopically large number of photogenerated charge carriers. The horizontal projections of the field cause in-layer transport (shown by thick arrows) of the carriers from the excitation spot.

The electric induction in the bilayer volume at the laser excitation spot is  $\mathbf{D} = \mathbf{E} + 4\pi\mathbf{P}$ . Here  $\mathbf{E} = E_0\mathbf{e}_z$  is the

static uniform electric field generated by  $V_g$  and  $\mathbf{P}$  is polarization of the medium. If  $n$  is the density of electron-hole pairs in the excitation spot of area  $S$  and  $d$  is the average distance between the pairs in different wells (i.e.,  $d$  is the dipole length), then  $\mathbf{P} = -(nS)(ed)/(Sd)\mathbf{e}_z = -(ne)\mathbf{e}_z$  and  $\mathbf{D} = (E_0 - 4\pi ne)\mathbf{e}_z$ . In the experiments [29] the DQW structure was considered as an insulator. It means that condition

$$E_0 \gg 4\pi en, \quad (1)$$

should be fulfilled in the excitation spot region. In this case the gate voltage results in a linear slope of the DQW potential energy profile along  $Z$  axis on the value  $\delta U(z) \approx -eE_0z$  (Fig. 1(right)).

However, at typical value  $V_g \approx 1$  V and  $n \sim 10^{10}\text{cm}^{-2}$  [29] one gets  $eE_0 \approx eV_g/(2L) \sim 10^4$  eV/cm, where  $L = 200$  nm is the width of external barrier of the DQW structure (Fig. 1(left)), and  $4\pi ne^2 \sim 10^4$  eV/cm. So at expected densities  $n \sim 10^{11} \div 10^{12}$   $\text{cm}^{-2}$  in the excitation spot at high pumping power, the condition (1) is not fulfilled there. It means that  $Z$ -axis component of the resulting field  $E_z$  is essentially dependent on  $z$  in the excitation spot region. More importantly, in this case there exists an in-plane component  $E_r$  of the electric field that will push both electrons in one layer and holes in another layer away from the excitation spot (Fig. 3).

### Second scenario: hot carrier transport induced by the repulsive in-layer interaction

If the photogenerated electrons and holes do not leave the excitation spot for any reason then the higher the pumping power  $P_{ex}$  the higher the carriers densities in the spot. (Since the excitation is off-resonant, the value of the exciton formation time is always larger than the time of energy relaxation of the carriers to reach the exciton transition.) Due to the bilayer geometry, there exists a value of excitation power at which the carrier densities in the spot reach the values when repulsive in-layer Coulomb forces between carriers become stronger than the attractive interlayer force. To be more specific, let us make an estimate of the interaction strength in the excitation spot through the dimensionless interaction parameter  $r_s$ . At small carrier densities the interaction in the spot is dipole-dipole one rather than the Coulomb as in the case of a monolayer. In particular, for electron (or hole) monolayer

$$r_s = (e^2/\bar{r})/(\hbar^2/(m\bar{r}^2)) = \bar{r}/a_B \sim 1/\sqrt{na_B^2}, \quad (2)$$

where  $a_B = \hbar^2/(me^2)$  is Bohr radius,  $n$  is the carrier density in the spot, and  $\bar{r} \sim n^{-1/2}$  is the average distance between carriers. Thus, for monolayer the increase of density  $n$  leads to the decrease of interaction. However,

in the case of electron-hole (e-h) bilayer at  $\bar{r} > d$ , where  $d$  is the interlayer distance, the interaction is dipole-dipole one,  $U = e^2 d^2 / \bar{r}^3$  rather than  $e^2 / \bar{r}$ . This leads to

$$r_s = U / (\hbar^2 / (m\bar{r}^2)) = d^2 / (\bar{r}a_B) \sim (d/a_B) \sqrt{nd^2}, \quad (3)$$

where  $n < n_c \lesssim d^{-2} \sim 10^{12} \text{ cm}^{-2}$  at  $d \sim 10^{-6} \text{ cm}$  [29]. It is seen that in this case the interaction increases in accord with the densities. At  $n = n_c$  (that corresponds to some *critical excitation power*  $(P_{ex})_c$ ) the character of interaction is changing: the repulsive in-layer interaction becomes dominating and, moreover, one should put  $n = 0$  effectively in the estimate (2), i.e., the repulsive interaction becomes huge. It leads to the appearance of in-layer electric fields ejecting the electrons and holes from the excitation spot region. Then the e-h densities in the spot grow to the critical values again and the ejection process recurs. There is a direct correspondence between this self-organized ejection, which keeps the critical values of carrier densities in the spot, and the avalanches in classical sand-pile model of SOC [28, 31].

Since the mobilities of charge carriers in GaAs QWs are very high (up to  $10^7 \text{ cm}^2/(\text{Vs})$  for electrons at sub-Kelvin temperatures [32–35]), the initial kinetic energies of some part of ejected particles can exceed the threshold of optical phonon emission. Their relaxation in energy is then very fast so these carriers will likely form excitons not far away from the excitation spot. In turn, the carriers with kinetic energy less than optical phonon energy  $\hbar\omega_{opt}$  go further. These carriers relax relatively slowly by emitting acoustic phonons. In GaAs  $\hbar\omega_{opt} \approx 37 \text{ meV}$  so the velocities of the carriers contributing to long-distance transport are less than  $v_{\text{max}} \sim 10^7 \text{ cm/s}$ . (Some more details about carrier energy relaxation due to phonon emission can be found in Appendix B.)

In addition, there is an essential difference in mobilities, and in effective masses, for electrons and heavy holes in GaAs [32–34]. This can lead to some difference in in-layer "stream" velocities of electrons and holes. The latter, in turn, would result in a suppression of the attractive interlayer Coulomb force (see Appendix C for details) until the velocities become small enough due to the acoustic phonon emission. In this conditions the interlayer exciton formation is also suppressed in some region of distances from the excitation spot. (Recall, for example, that the classical scattering cross-section for the Coulomb potential, the Rutherford cross-section, is proportional to  $V^{-4}$ , where  $V$  is the initial relative velocity at infinite distance.) The suppression leads naturally to the formation of a luminescence ring that would define a circumference of the total luminescence pattern.

Thus, the internal ring of luminescence (Fig. 2) might appear due to the electrons and holes that had emitted optical phonon(s) and then quickly formed excitons. In turn, the external luminescence ring can appear due to the carriers that were under the optical-phonon emission

threshold so they needed larger time (and corresponding distance) to relax emitting acoustic phonons.

In general, we suggest that at high photoexcitation power there exists an in-plane electric field  $E_r$  which consists of two contributions, "gate voltage-induced" and "in-layer interaction-induced". Due to high mobilities of charge carriers in GaAs even a moderate value of  $E_r$  results in high initial velocities of the carriers directed towards the outside of the excitation spot. Large relative velocities of the ejected electrons and holes lead to the suppression of the interlayer Coulomb attraction between them. The latter results in the suppression of exciton formation in some domain of distances from the excitation spot. In turn, the formation dynamics of ring-shaped luminescence pattern can be divided in three stages: (i) radial acceleration of carriers in the excitation spot region due to the in-plane component of the static electric field that appears at relatively high carrier density in the excitation spot and due to the in-layer Coulomb repulsion at high pumping power; (ii) slowing down of unbound carriers due to emission of optical and acoustic phonons and due to the ambipolar electric field ("Coulomb drag") (iii) the regime of strong interlayer Coulomb correlations - formation and optical recombination of interlayer excitons.

In what follows we are focused on the second scenario and test it by molecular dynamic (MD) simulations.

## MOLECULAR DYNAMICS SIMULATIONS: NUMERICAL MODEL

To describe the spatial dynamics of  $N$  hot electrons and holes, we use classical equations of motion

$$m_e^* \ddot{\mathbf{r}}_e^i + \gamma_e \dot{\mathbf{r}}_e^i = \sum_{j \neq i} \frac{e^2 (\mathbf{r}_e^i - \mathbf{r}_e^j)}{|\mathbf{r}_e^i - \mathbf{r}_e^j|^3} - \sum_k \frac{e^2 (\mathbf{r}_e^i - \mathbf{r}_h^k)}{[(\mathbf{r}_e^i - \mathbf{r}_h^k)^2 + d^2]^{3/2}}, \quad (4)$$

$$m_h^* \ddot{\mathbf{r}}_h^i + \gamma_h \dot{\mathbf{r}}_h^i = \sum_{j \neq i} \frac{e^2 (\mathbf{r}_h^i - \mathbf{r}_h^j)}{|\mathbf{r}_h^i - \mathbf{r}_h^j|^3} - \sum_k \frac{e^2 (\mathbf{r}_h^i - \mathbf{r}_e^k)}{[(\mathbf{r}_h^i - \mathbf{r}_e^k)^2 + d^2]^{3/2}}, \quad (5)$$

combined with the conditions of exciton formation and optical phonon emission (see below). Here vectors  $\mathbf{r}_e^i$  and  $\mathbf{r}_h^j$  are in-plane positions of  $i$ -th electron and  $j$ -th hole ( $1 \leq i, j \leq N$ ),  $m_{e(h)}^*$  is the electron (hole) effective mass,  $e$  is the electron charge, and  $d$  is the interlayer distance (see Fig. 4).

In addition to the inertia terms, the left-hand side of Eqs.(4-5) contains phenomenological momentum damping terms due to the interaction with acoustic phonons with constants  $\gamma_{e(h)} = e/\mu_{e(h)}$ , where  $\mu_{e(h)}$  is electron

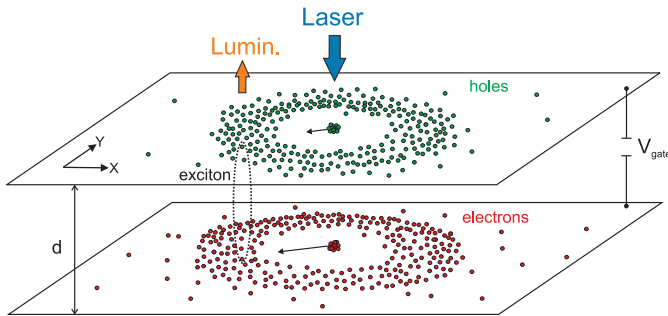


Figure 4: Qualitative schematic of optically-excited electron-hole bilayer. Both stationary laser pumping in the center and spatially-distributed luminescence are perpendicular to the layers. The charge separation between the layers postulated in the numerical model is due to the external gate voltage  $V_{gate}$ .

(hole) mobility. The dimensionless equations read

$$\ddot{\mathbf{r}}_e^i + \dot{\mathbf{r}}_e^i = \sum_{j \neq i} \frac{(\mathbf{r}_e^i - \mathbf{r}_e^j)}{|\mathbf{r}_e^i - \mathbf{r}_e^j|^3} - \sum_k \frac{(\mathbf{r}_e^i - \mathbf{r}_h^k)}{[(\mathbf{r}_e^i - \mathbf{r}_h^k)^2 + d^2]^{3/2}}, \quad (6)$$

$$\ddot{\mathbf{r}}_h^i + c_1 \dot{\mathbf{r}}_h^i = \sum_{j \neq i} \frac{c_2 (\mathbf{r}_h^i - \mathbf{r}_h^j)}{|\mathbf{r}_h^i - \mathbf{r}_h^j|^3} - \sum_k \frac{c_2 (\mathbf{r}_h^i - \mathbf{r}_e^k)}{[(\mathbf{r}_h^i - \mathbf{r}_e^k)^2 + d^2]^{3/2}}, \quad (7)$$

with constants  $c_1 = m_e^* \mu_e / (m_h^* \mu_h)$  and  $c_2 = m_e^* / m_h^*$ . Hereafter, we normalized time by  $t_e = \sqrt{\epsilon m_e^* \mu_e} / e$ , where  $\epsilon$  is dielectric constant of the layers, and all distances by  $\xi_e = \sqrt[3]{m_e^* \mu_e^2}$ . To estimate the parameters, we used well-known experimental values for high-quality undoped GaAs/AlGaAs QWs. In particular, taking typical  $\mu_e \sim 10^7 \text{ cm}^2/(\text{Vs})$  [32, 33] for temperatures  $T \lesssim 1 \text{ K}$ ,  $m_e^* \approx 0.067 m_e$ ,  $m_h^* \approx 0.5 m_e$  ( $m_e$  is bare electron mass),  $\epsilon = 12.8$  and  $\mu_h \sim 0.1 \mu_e$  [34], one gets  $t_e \sim 10^{-9} \text{ s}$ ,  $\xi_e \sim 10^{-4} \text{ cm}$ ,  $c_1 \sim 1$  and  $c_2 \sim 0.1$ .

The optical phonon emission was modeled in the following way: if the kinetic energy of a carrier exceeded the energy of optical phonon, the latter was subtracted from the first and the new direction of the carrier velocity became random.

**Simulation of the Laser Pumping.** Stationary optical pumping of carriers was simulated by generating them in random positions inside the excitation spot of radius  $r_0$  with some generation rate which was modeled in two different ways. In fact, during a MD simulation the time is changed by discrete steps, with the elementary time step  $\Delta t$ . According to the first way [25, 36], the generation rate  $p$  was defined as a probability per  $\Delta t$  to create *one* e-h pair in the excitation spot, so that  $p \Delta t < 1$ . We refer this case as *single generation regime (SGR)*. Alternatively, one can consider the formation of several e-h pairs during  $\Delta t$ . Then the carrier generation

rate (CGR) is defined as a number of e-h pairs generated in the excitation spot during the time step  $\Delta t$ . We call it as *multiple generation regime (MGR)*. Note that the results of MD simulations differ essentially in the single and multiple regimes. Indeed, it is intuitively clear that SGR likely corresponds to weak pumping whereas MGR describes high-power excitation.

The initial velocities of carriers in the excitation spot were also chosen randomly within intervals  $|\dot{\mathbf{r}}_e^i| \leq v_0$  and  $|\dot{\mathbf{r}}_h^i| \leq \eta v_0$ , where we took  $\eta = 0.5$  for all simulations.

During the spatial dynamics of the carriers, the exciton formation happened if an electron and a hole were close enough to each other,  $|\mathbf{r}_e - \mathbf{r}_h| < a$ , where  $a(d)$  is a phenomenological in-layer exciton radius, and their relative velocity was smaller than some critical value,  $|\dot{\mathbf{r}}_e - \dot{\mathbf{r}}_h| < V_c$  [25] (see also Appendix C). Note that the dependence of exciton formation rate on the e-h relative velocity is one of the most crucial ingredient for the ring-shaped pattern formation: assuming the absence of such dependence one always gets a spatially-monotonic decrease of the luminescence outside the excitation spot [25].

To simplify the simulations, we did not consider the exciton dynamics. It means that as soon as an electron and a hole had formed an exciton, their dynamics was no longer considered and the position of the formation event was recorded as a position of photon emission. Qualitatively, this corresponds to zero exciton lifetime.

One should note that since both the internal and external ring radii are temperature-independent [6, 29], it is not advisable to include temperature (i.e., to add a stochastic force in Eqs.(4-5)) in the consideration. In turn, since the low-temperature fragmentation of the external ring [6] apparently depends on the exciton dynamics, we do not expect to observe the fragmentation in the simulation results.

Finally, due to the inevitable restrictions in computational power it was only possible to simulate the dynamics of  $N \lesssim 10^4$  interacting particles. For this reason we had to modify the values of  $a$ ,  $v_0$ ,  $V_c$ ,  $d$  etc in comparison with realistic values to facilitate the exciton formation. However, it was clearly seen that the closer values of those model and real parameters, the better the correspondence between the MGR simulation results and the experimental ones. Note that the in-plane motion of the carriers was not restricted by any spatial boundaries.

## MOLECULAR DYNAMICS SIMULATIONS: RESULTS

Some preliminary results for the SGR have been published in Ref.[25]. In particular, quasi-1D simulations and the crucial dependence of the ring pattern formation on the critical relative velocity  $V_c$  in the exciton formation condition were discussed there. In what follows some new

essential results are described.

### Single generation regime (SGR)

The results of MD simulations of Eqs.(6-7) in the SGR for several sets of parameters indicate that there are two qualitatively different pictures. In general, the in-layer distribution  $n_{lum}(r)$  of stationary luminescence exhibits a ring-shaped pattern around the excitation spot. However, the pattern always contains only one ring. More importantly, the ring can originate by two qualitatively different ways.

According to the first way, the in-layer distributions of electrons and holes are separated from each other and the ring occurs in the region of their overlapping (Fig. 5).

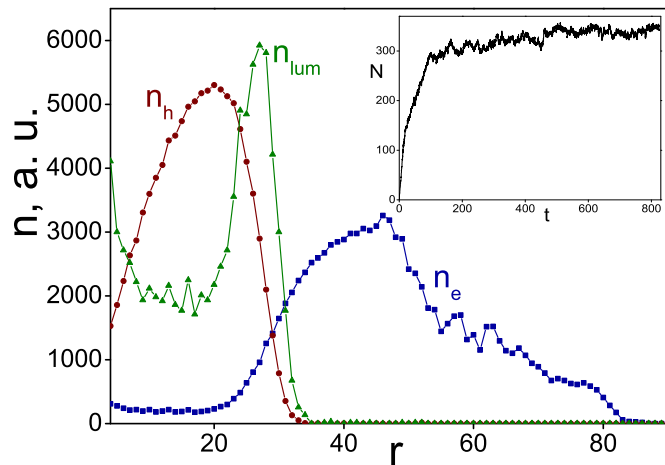


Figure 5: Stationary in-layer distributions of electrons ( $n_e$ ), holes ( $n_h$ ) and luminescence ( $n_{lum}(r)$ ) averaged over time interval (200,830). Inset: dependence of the total number  $N$  of electrons and holes on time  $t$ . In a stationary state the carrier generation rate is balanced by the luminescence rate so  $N(t)$  exhibits saturation. Parameters of the simulation: excitation spot radius  $r_0 = 4$ ,  $p = 10$ , velocity of optical-phonon emission threshold  $v_{opt} = 50$ , maximal electron initial velocity  $v_0 = 50$ , critical relative velocity  $V_c = 10$ , critical relative distance  $a = 0.2$ , first and second coefficients in the equations of motion for holes  $c_1 = 1$  and  $c_2 = 0.25$ ,  $d^2 = 0.01$ , time step  $\Delta t = 0.0005$ .

The dependence of the ring position on generation rate  $p$  (Fig. 6), which mimics the excitation power, shows that though the luminescence ring intensity increases with  $p$  its position is virtually independent on  $p$  (Top inset in Fig. 6). This behaviour differs from that observed experimentally (Fig. 2), where the radius of external luminescence ring grows near linearly with the increase of photoexcitation intensity and the growth of the internal ring radius is also quite noticeable. Interestingly, the

same behaviour, i.e., independence of the ring position on  $p$ , was observed in quasi-1D case [25].

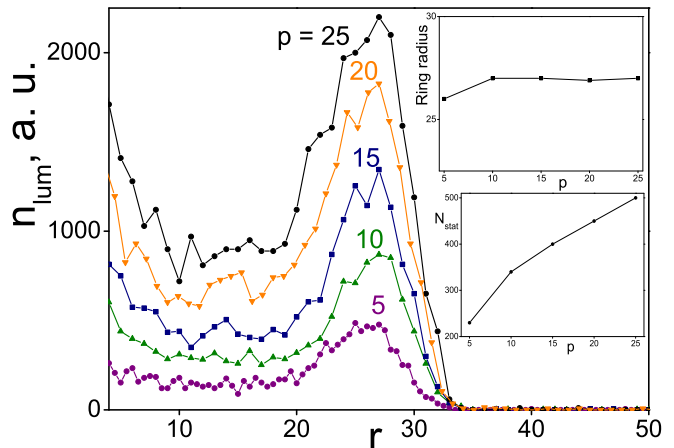


Figure 6: Dependence of stationary in-layer luminescence distribution  $n_{lum}(r)$  on generation rate  $p$ . Top inset: dependence of the luminescence ring radius on  $p$ . Bottom inset: stationary total number  $N_{stat}$  of electrons and holes vs  $p$ . Parameters of the simulations are the same as in Fig. 5.

However, there exists another way of the ring pattern formation. It was observable at other sets of parameters, in particular, when maximal initial velocities of the carriers, the critical relative velocity  $V_c$  and the distance  $a$  were relatively small. Note that the CGR  $p$  was taken in the same range of values as previously.

According to the second way, the in-layer distributions of electrons and holes practically coincide with each other (Fig. 7). The ring occurs at the outer side of the distributions, where the differences in the carrier densities and velocities are small enough to allow the exciton formation. The dependence of the ring radius on the CGR  $p$  (Fig. 8) has shown that, in contrast to the previous case (Figs. 5 and 6), the radius increases linearly with  $p$ .

Summarizing the simulation results for the SGR, one can conclude that the first way of the ring pattern formation, when electron and hole in-plane distributions are separated and the ring is formed at their overlapping, does not correspond qualitatively to the experimental results [6, 13, 24]. The second way could mimic the experimental situation when the excitation power was such that only the internal ring of luminescence was observable. However, the position of the ring in the simulations depends on the pumping rate stronger (linearly) than that of the internal ring (cp. Fig. 2 and Fig. 8) in the experiments [6, 13, 24]. In turn, nearly-linear dependence of the ring radius on the excitation power is typical for the external ring of luminescence (Fig. 2), but then the simulations omit the internal ring.

This misfit can indicate that though the parameters of the simulations in the second case are closer to realistic ones, one needs more realistic carrier generation

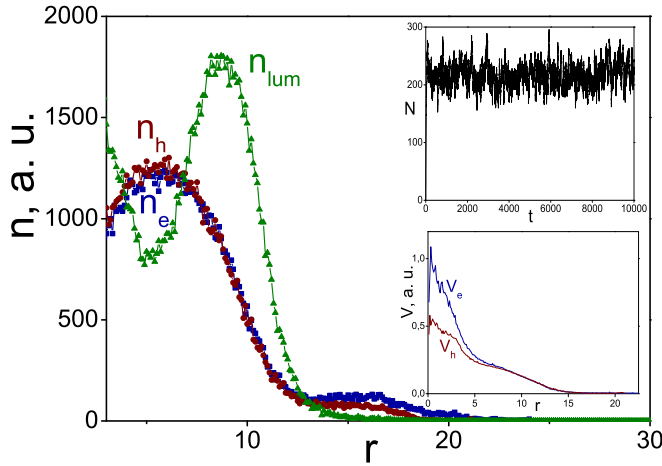


Figure 7: Stationary in-layer distributions of electrons ( $n_e$ ), holes ( $n_h$ ) and luminescence ( $n_{lum}(r)$ ) averaged over time interval (500,10000). Top inset: dependence of the total number  $N$  of electrons and holes on time  $t$  exhibits a stationary state. Bottom inset: dependence of electron ( $V_e$ ) and hole ( $V_h$ ) stream velocities vs distance  $r$  from the excitation spot center. Parameters of the simulation:  $r_0 = 3$ ,  $p = 10$ ,  $v_{opt} = 10$ ,  $v_0 = 1$ ,  $V_c = 1$ ,  $a = 0.05$ ,  $c_1 = 1.1$ ,  $c_2 = 0.3$ ,  $d^2 = 0.9$  (at smaller  $d^2$  the results are essentially the same), time step  $\Delta t = 0.005$ .

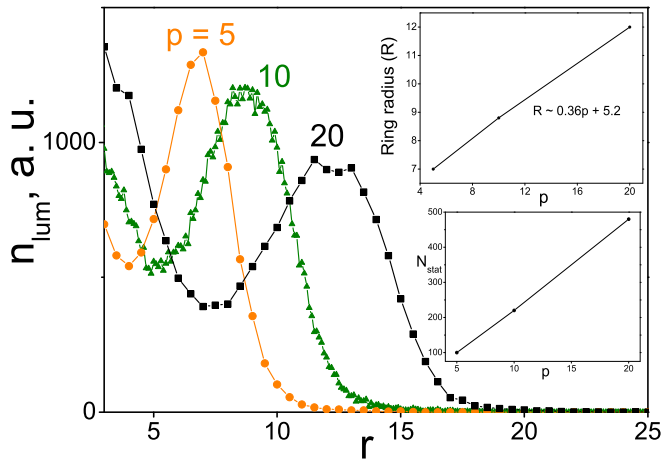


Figure 8: Dependence of stationary in-layer luminescence distribution  $n_{lum}(r)$  on generation rate  $p$ . Top inset: dependence of the luminescence ring radius on  $p$ . Bottom inset: stationary total number  $N_{stat}$  of electrons and holes vs  $p$ . Parameters of the simulations are the same as in Fig. 7.

algorithm which would enable us to model high excitation powers and, at the same time, is independent on the MD time step  $\Delta t$ .

## Multiple generation regime (MGR)

In the MGR the simulations result in much better correspondence with the experimental plots (Fig. 2) and, simultaneously, one can trace some correspondence with the SGR results ("the second way").

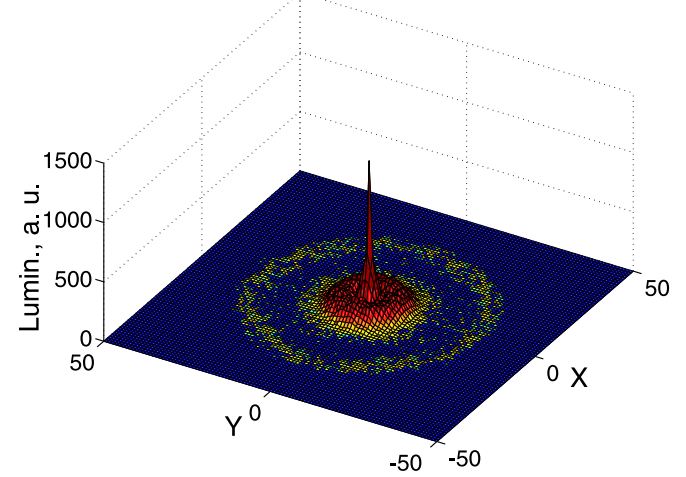
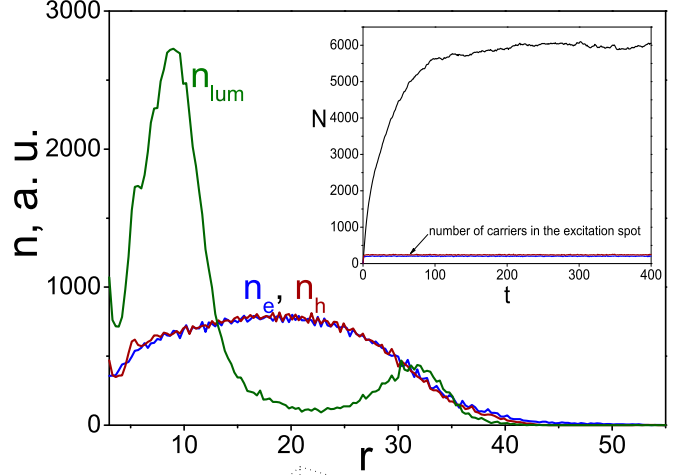


Figure 9: Top: Stationary in-layer distributions of electrons ( $n_e$ ), holes ( $n_h$ ) and luminescence ( $n_{lum}(r)$ ) averaged over time interval (100,400). Inset on top: dependence of the total number  $N$  of electrons and holes on time  $t$  exhibits stationary regime. Bottom: 3D luminescence pattern. Parameters of the simulation:  $r_0 = 3$ , pumping rate (number of particles generated during time step  $\Delta t$  in the spot)  $\Delta N_{spot} = 3$ ,  $v_{opt} = 10$ ,  $v_0 = 1$ ,  $V_c = 1$ ,  $a = 0.05$ ,  $c_1 = 1.1$ ,  $c_2 = 0.3$ ,  $d^2 = 0.9$ ,  $\Delta t = 0.01$ .

First, the MGR results show two concentric rings in the in-layer luminescence pattern: the internal ring has small radius and high intensity and the external ring has relatively large radius and is weaker in intensity (Fig. 9). The in-layer distributions of electrons and holes are similar to those of the above SGR "second way" (Fig. 7), i.e., the distributions practically coincide with each other.

Due to the increase of effective pumping power in the MGR case the total number of carriers in the stationary state (inset in Fig. 9) is more than one order of magnitude larger than that in the SGR case. Note that the stationary number of carriers in the excitation spot is very close to the product of instant CGR ( $\Delta N_{spot}/\Delta t = 300$ ) and the unit time. It means that most of the carriers escape from the spot very fast. This can be understood by making an estimate of the critical number of carriers in the spot required for dominant in-layer repulsion (see Section 2): taking  $n_c \sim d^{-2}$  one gets  $N_c = n_c \pi r_0^2 \sim \pi (r_0/d)^2 \approx 30$ , which is much smaller than the above number of carriers formed in the spot during the unit time. (For the estimate we have used the parameters in Fig. 9 caption.) Thus, the system of charge carriers is in the critical state.

The mechanism of the ring pattern formation in these conditions is as follows. The internal ring is formed due to the carriers which have emitted optical phonons. It can be seen in Fig. 10 by the sharp changes of carrier velocities within the excitation spot. Note that the velocities essentially exceed the maximal initial velocities there. (In addition, the optical phonon emissions were seen during the simulations by changes of instant maximal velocities of the carriers that were up to the threshold velocity of optical phonon emission.) It means that the in-layer repulsive Coulomb interaction is dominant in the excitation spot. The repulsive forces accelerate the carriers so that the major part of them emits optical phonons and then quickly forms excitons. The carriers with velocities beneath the threshold velocity of optical phonon emission go further emitting acoustic phonons and, eventually, form excitons relatively far away from the excitation spot. This description is in excellent agreement with all sets of simulations in the MGR so it justifies the second scenario suggested in Section 2. Some details of the Coulomb repulsion accompanied by phonon emission are given in Appendix B.

To prove the crucial role of Coulomb interactions, we have performed the simulation where the interactions are switched off even though the exciton formation condition holds. The results are shown in Fig. 11. One can see that the saturation of  $N(t)$  (i.e., the stationary state) is absent during the time which essentially exceeds previous simulation times for the MGR. The in-layer distributions of electrons and holes resemble those for the "first way" SGR, i.e., there is spatial separation of the distributions. However, the ring does not form and the luminescence decreases monotonically from the center.

Let us now discuss the dependence of the ring-shaped pattern on (i) pumping power and (ii) critical relative velocity  $V_c$  from the exciton formation condition.

The dependence of in-plane positions of the rings on the pumping rate is shown in Fig. 12. The external ring radius increases nearly linearly whereas the internal ring radius grows more slowly. This behaviour exhibits a good

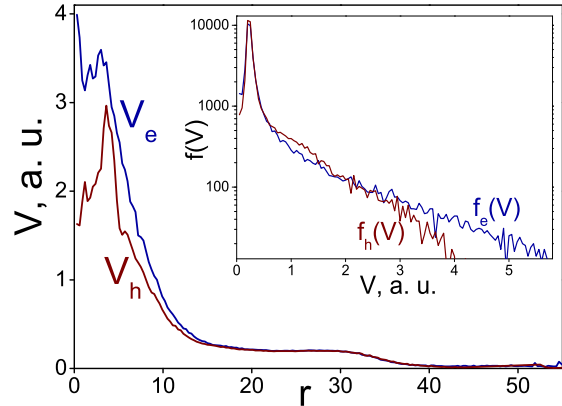


Figure 10: Dependence of electron ( $V_e$ ) and hole ( $V_h$ ) stream velocities vs distance  $r$  from the excitation spot center. One can see that the carrier velocities within the excitation spot region essentially exceed the maximal initial velocity ( $= 1$ ). Note that  $V_e$  and  $V_h$  are the velocities of that part of the carriers which are below threshold of optical phonon emission. Inset: Electron ( $f_e(V)$ ) and hole ( $f_h(V)$ ) distributions over single-particle velocities. Parameters of the simulation are the same as in Fig. 9.

agreement with the experimental curves (Fig. 2). (To determine the dependences more accurately one needs to collect larger statistics that is a very time-consuming procedure due to the large total numbers ( $\sim 10^4$ ) of particles in the MGR.)

The dependence of the ring-shaped luminescence pattern on the critical relative velocity  $V_c$  shows (Fig. 13) that the smaller  $V_c$  the larger the external ring radius (top inset in Fig. 13) and the ring intensity. At the same time the stationary number of carriers grows up to the limiting values of order of  $10^4$  (bottom inset in Fig. 13) for the available computational power.

Finally, we have performed simulations with two identical but spatially separated excitation spots to compare our results (see Fig. 14) with experimental pictures [13, 30]. One can see that when the spots are placed close enough, the external rings open towards each other forming a figure similar to one of the Cassini ovals. This behaviour also corresponds to the experiments even though the simulations do not include the exciton dynamics.

Summarizing the simulation results for the MGR, we conclude that they show reasonable correspondence with the experiments [6, 13, 24, 30]. Therefore the theoretical explanations [13, 14, 16–18, 24] of the ring pattern formation based on the diffusion-induced spatial separation of in-layer distributions of electrons and holes (see Appendix A) must be revised.



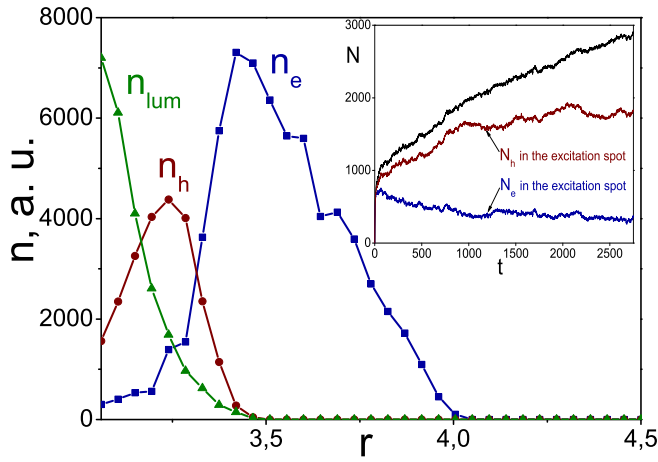


Figure 11: In-layer distributions of electrons ( $n_e$ ), holes ( $n_h$ ) and luminescence ( $n_{lum}(r)$ ) averaged over time interval (1500,2700) in the absence of any direct Coulomb interactions. Inset: dependence of the total number  $N$  of electrons and holes on time  $t$ . It shows that the dynamics is still non-stationary. Parameters of the simulation are the same as in Fig. 9.

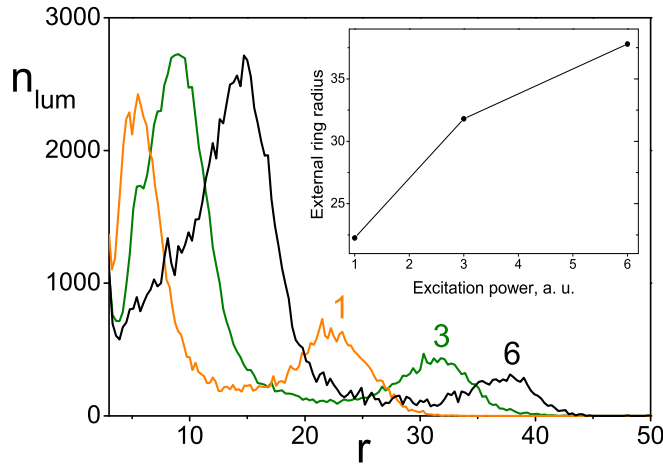


Figure 12: Dependence of stationary in-layer luminescence distribution  $n_{lum}(r)$  on excitation power with the number  $\Delta N_{spot}$  of particles generated per time step in the spot shown by numbers (1, 3, 6) near the corresponding curves. Inset: dependence of the external ring radius on excitation power. Other parameters of the simulations are the same as in Fig. 9.

## CONCLUSION AND DISCUSSION

It has been shown that the stationary ring-shaped luminescence pattern forms due to the hot carrier transport (HCT) caused by the in-plane electric fields which appear at high enough excitation power in the excitation spot region. The HCT is essentially non-diffusive. In particular, the internal luminescence ring appears due to electrons

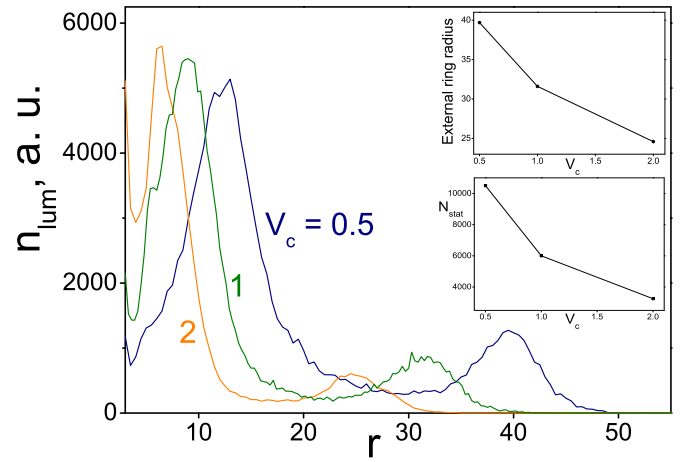


Figure 13: Dependence of stationary in-layer luminescence distribution  $n_{lum}(r)$  on critical relative velocity  $V_c$  from the exciton formation condition. Top inset: dependence of the external ring radius on  $V_c$ . Bottom inset: stationary total number  $N_{stat}$  of carriers vs  $V_c$ . The pumping rate  $\Delta N_{spot} = 3$ . Other parameters of the simulations are the same as in Fig. 9.

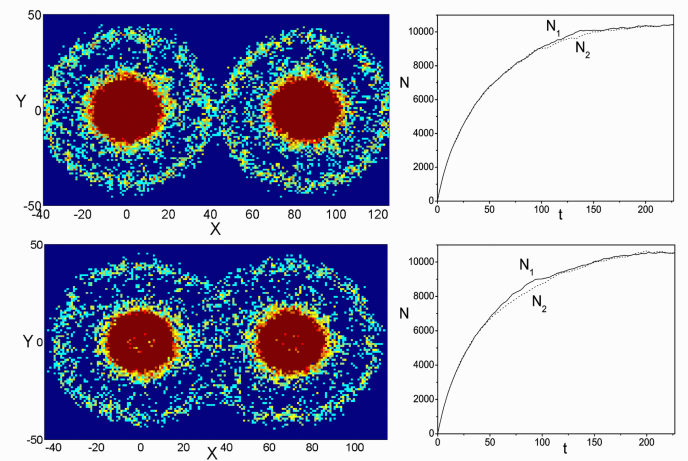


Figure 14: Left: Luminescence patterns for the case of two excitation spots at two different distances, 85 (top) and 70 (bottom), between the spots. Right: Corresponding dependences of total numbers  $N_{1,2}$  of carriers excited by the spots on time  $t$  show that the system arrives at the stationary state. Parameters of the simulations are the same as in Fig. 9 except critical relative velocity, here  $V_c = 0.5$ .

and holes emitted optical phonons whereas the external ring forms due to the relaxation of carriers, which are initially below the threshold of optical phonon emission. To form excitons, these carriers relax emitting acoustic phonons and, in addition, due to the interlayer Coulomb drag.

The ring-shaped pattern formation is particularly interesting as a possible bright signature of self-organized

criticality [28, 31]. Though "the second scenario" naturally involves the SOC regime, the MGR simulations reported have been performed in the critical state. So the transition to the SOC regime as well as its statistical properties (1/f-noise etc) are still open questions.

The author thanks L. P. Paraskevova for the encouragement, and Yu. M. Kagan and F. V. Kusmartsev for helpful discussions.

## APPENDIXES

### Appendix A: Diffusive model of charge carrier transport

The diffusive transport model [13] used to explain the experiments [6] was based on two reaction-diffusion equations

$$\dot{n}_e = D_e \nabla^2 n_e - w n_e n_h + J_e(r), \quad (8)$$

$$\dot{n}_h = D_h \nabla^2 n_h - w n_e n_h + J_h(r). \quad (9)$$

Here  $n_e$  and  $n_h$  are electron and hole two-dimensional (2D) densities,  $w$  is electron-hole binding rate to form an exciton. The source term  $J_h(r) = P_{ex} \delta(\mathbf{r})$  for photoexcited holes is focused in the local excitation spot. The density of photoexcited electrons is supposed to be negligible in comparison with equilibrium electron density  $n_\infty$  in the absence of laser excitation. When  $n_\infty$  is spatially disturbed due to the presence of holes, there appears electron current  $J_e(r) = I - a \cdot n_e(r)$  spread in the quantum-well plane. Here  $I$  and  $a \cdot n_e$  are the currents in and out of the system such that  $n_\infty = I/a$ . (Note that  $a$  here is not the critical relative distance used in the simulations but an independent parameter.) Implying the stationary regime and the symmetry over the polar angle, and neglecting the exciton diffusion [15], one gets the exciton PL intensity  $I_{PL}(r) \propto n_e(r)n_h(r)$ .

Authors of Ref.[13] have assumed that a luminescence ring with radius  $R$  appears at the overlap of the electron and hole densities (see Fig. 15) so that  $n_h \gg n_e$  at  $r < R$  and  $n_h \ll n_e$  at  $r > R$  with  $n_e(r \rightarrow \infty) = n_\infty$  (Fig. 15). Neglecting the exciton formation term  $w n_e n_h$  far from the boundary  $r = R$ , one gets for holes

$$\nabla^2 n_h \equiv \frac{d^2 n_h}{dr^2} + \frac{1}{r} \frac{dn_h}{dr} = -(P_{ex}/D_h) \delta(\mathbf{r}). \quad (10)$$

Using boundary condition  $n_h(r = R) = 0$  it results in

$$n_h(r \leq R) = \frac{P_{ex}}{2\pi D_h} \ln\left(\frac{R}{r}\right). \quad (11)$$

For electrons one gets

$$\nabla^2 n_e = -(I/D_e) + (a/D_e) \cdot n_e(r)$$

with boundary conditions  $n_e(r = R) = 0$ ,  $n_e(r \rightarrow \infty) = n_\infty$ .

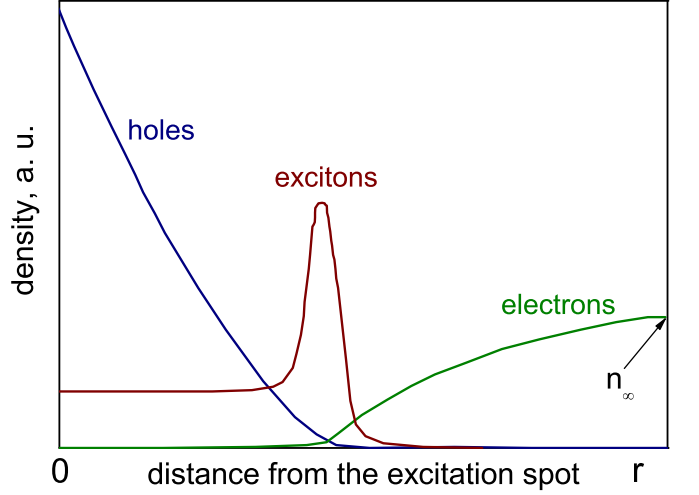


Figure 15: The density distributions (the scales are in a.u.) obtained in Ref.[13] with the use of the diffusive transport model described in text.

Denoting  $\Delta = (n_e - n_\infty)/n_\infty$  and  $x = r/\lambda$ , where  $\lambda \equiv \sqrt{D_e/a} = \sqrt{D_e n_\infty/I}$  is a characteristic length, we arrive at

$$\frac{d^2 \Delta}{dx^2} + \frac{1}{x} \frac{d\Delta}{dx} - \Delta = 0. \quad (12)$$

The last equation is the modified Bessel equation of zero order. The solution is

$$\Delta(x) = A \cdot K_0(x), \quad (13)$$

where  $A$  is some constant and  $K_0(x)$  is modified Hankel (or MacDonald) function of zero order, such that  $K_0(x \rightarrow 0) \approx \ln \frac{1}{x}$ ,  $K_0(x \rightarrow \infty) = 0$ . Thus,

$$n_e(r)/n_\infty = 1 + A \cdot K_0(r/\lambda). \quad (14)$$

If  $\lambda \gg R$ , as supposed in [13], then at  $R < r \ll \lambda$  the electron density  $n_e(r)/n_\infty \approx 1 + A \ln(\lambda/r)$ . Using the boundary condition  $n_e(r = R) = 0$  one finds coefficient  $A$ . Finally,

$$n_e(R < r \ll \lambda) \approx n_\infty [1 - \ln(\lambda/r) / \ln(\lambda/R)]. \quad (15)$$

Then it has been assumed that at the boundary between the electron and hole densities the total current is zero, i.e.,

$$D_e \frac{\partial n_e}{\partial r} \Big|_{r=R} = -D_h \frac{\partial n_h}{\partial r} \Big|_{r=R}. \quad (16)$$

From here it follows that

$$D_e n_\infty / \ln(\lambda/R) = P_{ex} / 2\pi, \quad (17)$$

so the ring radius can be expressed as

$$R = \lambda \exp(-2\pi D_e n_\infty / P_{ex}). \quad (18)$$

If one puts  $D_h = 0$ , the ring radius  $R$  must be equal to zero since according to the model the diffusion of holes is the only reason why they move out of the excitation spot. However, Eq.(18) does not depend on  $D_h$  so the ring radius is not zero at  $D_h = 0$ , i.e. the ring exists even if all holes are left into the excitation spot ( $D_h = 0$ ). This clearly unphysical result is not a consequence of the limiting case  $\lambda \gg R$ , but rather comes from wrong initial assumptions. (In Ref.[17] the result Eq.(18) has been generalized but even then  $R$  does not depend on  $D_h$ .)

Note that in the original paper [13] the erroneous formula for  $R$  has been given [27]:

$$R_{orig} = \lambda \exp(-2\pi D_e n_\infty / (D_h P_{ex})). \quad (19)$$

The presence of  $D_h$  in the exponent denominator could be deceiving since at first sight (i.e., without dimensionality check:  $[D_e] = [D_h] = \text{cm}^2/\text{s}$ ,  $[n_\infty] = \text{cm}^{-2}$ ,  $[P_{ex}] = \text{s}^{-1}$ ) it looked reasonable.

In addition, both the DTM [13] and its modifications [14, 16–18] could not explain in principle why the external luminescence ring appears only when the excitation power exceeds some critical value.

Nevertheless, the drift-diffusion regime can be applicable for slow charge carriers near the luminescence ring at  $r \sim R$ . (As before, we do not consider equilibrium carriers and are only focused on photogenerated ones.) In particular, the continuity equations in this regime are given by

$$\dot{n}_{e(h)} + \text{div } \mathbf{i}_{e(h)} = g_{e(h)} - \Gamma, \quad (20)$$

$$\dot{n}_X + \text{div } \mathbf{i}_X = \Gamma - n_X/\tau_X. \quad (21)$$

Here  $n_e$ ,  $n_h$  and  $\mathbf{i}_e = -n_e \mu_e \mathbf{E} - D_e \nabla n_e$ ,  $\mathbf{i}_h = n_h \mu_h \mathbf{E} - D_h \nabla n_h$  are 2D densities and particle flux densities of uncoupled electrons in plane  $z = d/2$  and holes in plane  $z = -d/2$ ,  $\mu_{e(h)}$  is electron (hole) mobility. The particle flux density for excitons  $\mathbf{i}_X \approx -D_X \nabla n_X$ , where  $n_X$  is the interlayer exciton density. The contribution from the dipole-dipole interaction between the excitons is omitted in  $\mathbf{i}_X$  since it appears as an above-linear correction on  $n_X$ . The carrier generation rates  $g_{e(h)}(\mathbf{r}, t)$  are some given functions. The exciton formation rate can be written as (hereafter inessential constant prefactors are dropped)

$$\Gamma(\mathbf{r}, t) = \int w(|\mathbf{v}_1 - \mathbf{v}_2|) f_e(\mathbf{r}, \mathbf{v}_1, t) f_h(\mathbf{r}, \mathbf{v}_2, t) d^2 \mathbf{v}_1 d^2 \mathbf{v}_2, \quad (22)$$

where  $f_{e(h)}(\mathbf{r}, \mathbf{v}, t)$  is the electron (hole) distribution function, so that  $n_{e(h)}(r, t) = \int f_{e(h)}(r, \mathbf{v}, t) d^2 \mathbf{v}$ , and  $w(v)$  is the specific exciton formation rate. The exciton lifetime  $\tau_X$  is supposed to be density-independent. Finally, the Poisson equation for the electric field reads

(time dependence is dropped;  $\varepsilon$  is dielectric constant)

$$\text{div}(\varepsilon \mathbf{E}(r, z)) = 4\pi e[(n_h(r) + n_X(r)) \delta(z + d/2) - (n_e(r) + n_X(r)) \delta(z - d/2)]. \quad (23)$$

It includes the contribution of the interlayer exciton dipole fields and keeps the electroneutrality for the free carrier system when the exciton formation is suppressed ( $n_X(r) = 0$ ).

At  $r \sim R$  one can put  $w(v) \approx w_{\max}$ , then  $\Gamma(r) \approx w_{\max} n_e(r) n_h(r)$  and the Eqs.(20),(21),(23) with  $g_{e(h)} = 0$  become a closed system.

Note that the ambipolar electric field  $\mathbf{E}$  might play an important role in the formation of a sharp intensity profile of the external luminescence ring. In this regard it is useful to note that the FWHM of the external ring intensity is almost independent on the ring radius  $R$  at high excitation powers (see Fig. 2).

## Appendix B

If  $e^2 \sqrt{n} > \hbar \omega_{opt}$  at  $n > d^{-2}$  the in-layer Coulomb repulsion in the excitation spot might be "exhausted" at small distances: the potential energy of the carriers transforms into kinetic one which, in turn, is spent for the fast optical phonon emission so that the carriers do not go far from the excitation spot.

To estimate whether the values of carrier densities in the excitation spot are sufficient for such process, let us consider two electrons resting at distance  $r_0$  from each other at moment  $t = 0$ . We neglect the energy dissipation due to acoustic phonon emission now to facilitate the effect described above. Then the equation of motion is

$$m\ddot{r} = e^2/r^2,$$

with  $m = m_e^*/2$ ,  $r = |\mathbf{r}_1 - \mathbf{r}_2|$ . (Dielectric constant  $\varepsilon$  is introduced by  $e^2 \rightarrow e^2/\varepsilon$  in the final expression.) The solution is expressed through the inverse function,

$$t/t_0 = \sqrt{x^2 - x} + \frac{1}{2} \ln \left( x + \sqrt{x^2 - x} \right),$$

where  $x = r/r_0$ ,  $t_0 = \sqrt{mr_0^3/(2e^2)}$ . At  $t > (3 \div 4)t_0$  with a good precision the velocity  $v \approx v_\infty = r_0/t_0$ , i. e., the electrons move near uniformly at large times. The condition of optical phonon emission reads

$$mv^2/2 = e^2/r_0 - e^2/r \geq \hbar \omega_{opt},$$

from where it follows

$$r \geq r_c = \frac{r_0}{1 - \hbar \omega_{opt}/(e^2/r_0)}.$$

Substituting  $r_0 \sim n^{-1/2}$  in the expression for  $r_c$ , one has

$$n \sim (\varepsilon \hbar \omega_{opt}/e^2 + 1/r_c)^2$$

The value  $n_c^* = (\varepsilon \hbar \omega_{opt}/e^2)^2 \approx 4 \cdot 10^{13} \text{ cm}^{-2}$  ( $\varepsilon \approx 12.8$ ,  $\hbar \omega_{opt} \approx 37 \text{ meV}$  for GaAs) at  $r_c = \infty$  is the smallest density at which the process of optical phonon emission is dominant. Note that at  $n > n_c^*$  the effect is extremely pronounced, e.g., at  $n = 1.003n_c^*$  (extra 0.3% to  $n_c^*$ ) one gets  $r_c \approx 1 \mu\text{m}$ . At  $n = n_c^*$  one gets  $r_0 \sim 0.1a_B$  for GaAs.

To find a qualitative dependence of carrier flux velocity on in-plane coordinates when the carrier kinetic energies are below the threshold of optical phonon emission, let us consider the previous model adding the dissipation due to acoustic phonons. Then for two electrons one has

$$\begin{aligned} m_e^* \ddot{\mathbf{r}}_1 &= e^2/|\mathbf{r}_1 - \mathbf{r}_2|^2 - \gamma \dot{\mathbf{r}}_1, \\ m_e^* \ddot{\mathbf{r}}_2 &= e^2/|\mathbf{r}_1 - \mathbf{r}_2|^2 - \gamma \dot{\mathbf{r}}_2, \end{aligned}$$

where  $\gamma = e/\mu_e$  is dissipation coefficient and  $\mu_e$  is electron mobility. Substituting  $\mathbf{R} = (\mathbf{r}_1 + \mathbf{r}_2)/2$  and  $\mathbf{r} = \mathbf{r}_1 - \mathbf{r}_2$ , in the center-of-mass frame ( $\dot{\mathbf{R}} = 0$ ), the equation of motion reads

$$m \ddot{r} = e^2/r^2 - \frac{1}{2} \gamma \dot{r}.$$

The dissipation of energy  $E(r) = mv^2(r)/2 + e^2/r$  is given by  $dE/dr = -\gamma v(r)/2$  (since  $dE/dt = -\gamma v^2/2$ ) that leads to equation

$$mv(r) \frac{dv}{dr} = \frac{e^2}{r^2} - \frac{1}{2} \gamma v(r).$$

In the dimensionless form ( $r = r_0 x$ ,  $v = v_\infty u$ ) one gets

$$u(x) \left[ \frac{du}{dx} + a \right] = \frac{1}{2x^2}, \quad (24)$$

where parameter  $a = \sqrt{\gamma^2 r_0^3 / (8me^2)}$ ,  $x \geq 1$  and  $u(x=1) = 0$ . (To avoid a confusion, note again that this  $a$  has its own meaning.) Using relation  $\gamma = e/\mu_e$ , one can rewrite the parameter as  $a = \frac{1}{2} (r_0/\xi_e)^{3/2}$ , where  $\xi_e = \sqrt[3]{m_e^* \mu_e^2}$  is characteristic length scale. Taking for GaAs  $\xi_e \sim 1 \mu\text{m}$  (see the description of the numerical model in the main text) and  $r_0 \sim n_c^{-1/2} \sim d \sim 10^{-6} \text{ cm}$ , one gets  $a \sim 10^{-3}$ . The equation (24) can be reduced to the Abel equation of the second kind. Its exact analytical solution is unknown. However, a qualitative behaviour of  $u(x)$  can be found from asymptotic solutions at  $x \rightarrow 1$  and  $x \rightarrow \infty$  (see also numerical solutions in Fig. 16). It is natural to assume that velocity  $u(x=\infty) = 0$ . So  $du/dx$  can be dropped in Eq. (24) at  $x \rightarrow \infty$  that gives  $u_\infty(x) \approx 1/(2ax^2)$ . Let us now rewrite Eq. (24) as

$$\frac{du}{dx} = \frac{1}{2x^2 u} - a.$$

At  $x \rightarrow 1$  due to the initial condition  $u \rightarrow 0$  so now the last term in the right-hand side can be dropped. It gives  $u_1(x) \approx \sqrt{1-1/x}$  at  $x \approx 1$ . The dependence of  $u(x)$  on  $a$  is as follows: the larger  $a$  the narrower the width of the

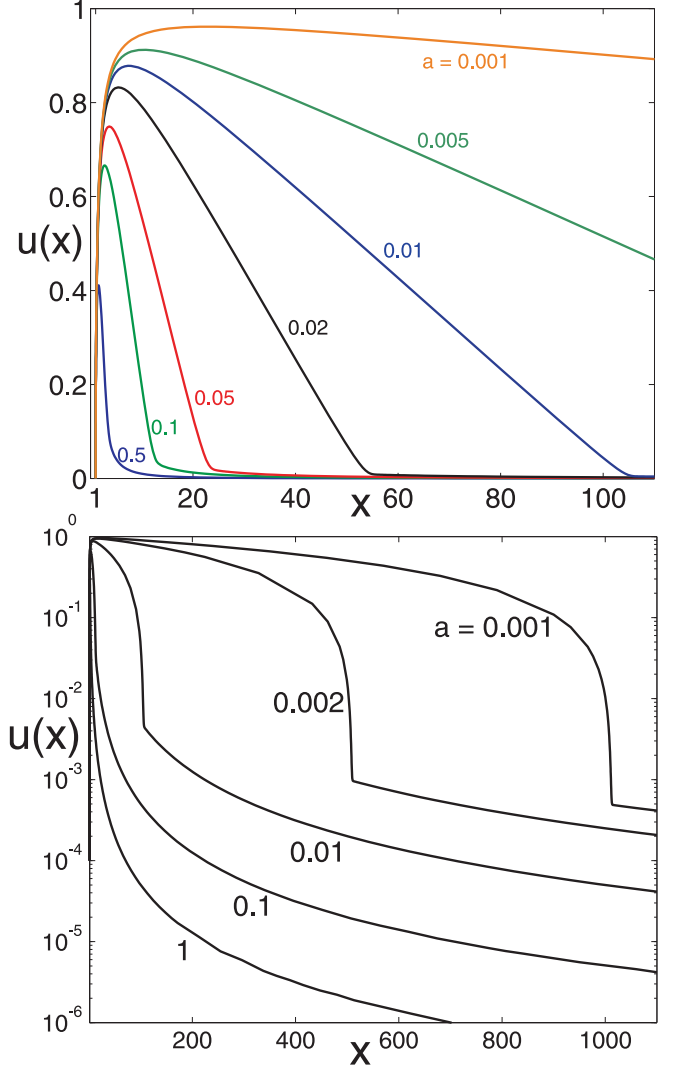


Figure 16: Numerical solutions of Eq. (24) with  $u(x) = v/v_\infty$  and  $x = r/r_0$  for different values of parameter  $a$ . Top: Linear scale. Bottom: Log scale.

peak and the smaller its height (see Fig. 16). Note that in the laboratory frame  $v_{e,h} = v/2$ ,  $r_{e,h} = r/2$ .

It is also interesting to note that the MGR simulations indicate that the external luminescence ring appears only if the carrier stream velocities  $V_{e(h)}(r)$  as functions of distance  $r$  from the excitation spot (see Fig. 10) have a non-monotonic dependence similar to that in Fig. 16, i.e., at small  $r$  the velocities grow reaching the maximal values at some finite  $r$  (often within the excitation spot region) and then they decrease to zero at large  $r$ .

### Appendix C: Suppression of exciton formation in the bilayer at high e-h relative velocity

Here we would like to illustrate how the critical relative velocity  $V_c$  appears in principle in the exciton formation condition. We can distinguish two mechanisms referred further as "geometric" and "kinetic" ones which lead to the existence of the critical e-h relative velocity above which the interlayer exciton formation is strongly suppressed.

**1. "Geometric" mechanism.** Due to the bilayer geometry, at sufficiently large relative e-h velocity the interlayer Coulomb attraction, which results in an exciton formation, is suppressed. To show this, let us consider the Fourier transform  $U_q = \int d^2\mathbf{r} \exp(i\mathbf{q}\mathbf{r}) U(r)$  of the pair interaction potential  $U(r) = -e^2/\sqrt{r^2 + d^2}$  between an electron from one layer and a hole from another ( $r$  is in-plane relative distance). One gets

$$U_q = -2\pi e^2 \int_0^\infty \frac{J_0(qr) r dr}{\sqrt{r^2 + d^2}} = -\frac{2\pi e^2}{q} \exp(-qd), \quad (25)$$

the "screened Coulomb" in the momentum representation. (The effects of charge screening studied in random phase approximation [37] lead to the change of the pre-exponential factor, which is not important in this consideration.) Thus, if the electron-hole relative velocity  $V = \hbar q/m > V_c = \hbar/(md)$ , the interaction between the carriers decreases exponentially with the increase of  $V$ . It means that one can neglect the interaction as well as the exciton formation at  $V > V_c$ . At  $d \approx 10^{-6}$  cm [29] and reduced e-h mass  $m \approx 0.06m_e$  in GaAs, one gets  $V_c \approx 3 \cdot 10^7$  cm/s, that is the same order of magnitude as threshold velocity  $v_{max}$  of optical phonon emission in GaAs ( $v_{max}/V_c \approx 1.5$ ).

**2. "Kinetic" mechanism.** The second mechanism is based on the fact that to form an exciton the unbound electron-hole pair must emit acoustic phonon. (Here we suppose that the carrier velocities are below the threshold of optical phonon emission.)

To illustrate this, let us consider a model system: an infinite train of electrons separated from each other by distance  $L$  uniformly moves with velocity  $V$  along a thread and an immovable hole is located at distance  $d$  from the thread. The interaction potential between the electron train and the hole as a function of time reads

$$U(t) = - \sum_{k=-\infty}^{+\infty} \frac{e^2}{\rho_k},$$

where  $\rho_k = \sqrt{(kL + Vt)^2 + d^2}$ . Although the sum diverges as  $1/|k|$ , the relative value of the potential  $\delta U(t) = U(t) - U(0)$  is convergent. The components of the corresponding force acting on the hole along and perpendicu-

lar to the thread are given by

$$F_{\parallel}(t) = \sum_{k=-\infty}^{+\infty} \frac{e^2 (kL + Vt)}{\rho_k^3}, \quad F_{\perp}(t) = \sum_{k=-\infty}^{+\infty} \frac{e^2 d}{\rho_k^3}.$$

Both the potential and the force are periodic functions of time with period  $T = L/V$ , e.g.,  $\delta U(t+T) = \delta U(t)$ .

In 2D case when there exists relative flow (with velocity  $V$ ) of electrons in one layer and holes in another, the interlayer interaction potential between the electron flow and a given hole oscillates with frequency  $\omega \sim V\sqrt{n}$ , where  $n$  is 2D density of electrons in the flow. If this frequency is higher than  $\tau^{-1}$ , where  $\tau = \min(\tau_{e-ac}, \tau_{h-ac})$  is the minimal carrier-acoustic phonon scattering time, the exciton formation in real space is not possible. Thus, one can write the condition of exciton formation as follows

$$V < V_c \sim 1/\sqrt{n\tau^2}. \quad (26)$$

If the carrier densities are essentially different, one should take  $n = \max(n_e, n_h)$  in (26). At  $n \sim 10^{10}$  cm $^{-2}$  and  $\tau \sim 10^{-9}$  s the critical relative velocity is  $V_c \sim 10^4$  cm/s.

In fact, one can get the estimate (26) in a more simple way. Let us suppose for definiteness that locally  $n_e > n_h$ . Then an e-h pair with relative velocity  $V$  can form an exciton if

$$V\tau < \bar{r}_{e-e} \sim n_e^{-1/2},$$

that is the electron or the hole should have time to emit an acoustic phonon before the next electron would come to the hole. The condition (26) follows directly from the latter formula.

- 
- [1] S. A. Moskalenko, Sov. Phys. Solid State **4**, 199 (1962).
  - [2] L. V. Keldysh, A. N. Kozlov, Sov. Phys. JETP **27**, 521 (1968).
  - [3] T. Fukuzawa, E. E. Mendez and J. M. Hong, Phys. Rev. Lett. **64**, 3066 (1990).
  - [4] L. V. Butov *et al.*, Phys. Rev. Lett. **73**, 304 (1994).
  - [5] Yu. E. Lozovik and O. L. Berman, JETP **84**, 1027 (1997).
  - [6] L. V. Butov, A. C. Gossard and D. S. Chemla, Nature **418**, 751 (2002).
  - [7] D. Snoke *et al.*, Nature **418**, 754 (2002).
  - [8] A. V. Larionov and V. B. Timofeev, JETP Letters **73**, 301 (2001).
  - [9] A. V. Larionov *et al.*, JETP Letters **75**, 570 (2002).
  - [10] D. Snoke *et al.*, Solid State Commun. **127**, 187 (2003).
  - [11] J. P. Eisenstein, A. H. MacDonald, Nature **432**, 691 (2004).
  - [12] A. V. Balatsky, Y. N. Joglekar and P. B. Littlewood, Phys. Rev. Lett. **93**, 266801 (2004).
  - [13] L. V. Butov *et al.* Phys. Rev. Lett. **92**, 117404 (2004).
  - [14] R. Rapaport *et al.*, Phys. Rev. Lett. **92**, 117405 (2004).
  - [15] L. S. Levitov, B. D. Simons and L. V. Butov, Phys. Rev. Lett. **94**, 176404 (2005).

- [16] S. Denev, S. H. Simon and D. W. Snoke, *Solid State Commun.* **134**, 59 (2005).
- [17] M. Haque, *Phys. Rev. E* **73** 066207 (2006).
- [18] A. A. Chernyuk, V. I. Sugakov, *Phys. Rev. B* **74**, 085303 (2006).
- [19] M. H. Szymanska, J. Keeling and P. B. Littlewood, *Phys. Rev. Lett.* **96**, 230602 (2006).
- [20] V. B. Timofeev and A. V. Gorbunov, *J. Appl. Phys.* **101**, 081708 (2007).
- [21] Sen Yang *et al.*, *Phys. Rev. B* **75**, 033311 (2007).
- [22] M. Stern *et al.*, *Phys. Rev. Lett.* **101**, 257402 (2008).
- [23] J. Kasprzak *et al.*, *Nature* **443**, 409 (2006).
- [24] Sen Yang *et al.*, *Phys. Rev. B* **81**, 115320 (2010).
- [25] A. V. Paraskevov and S. E. Savel'ev, *Phys. Rev. B* **81**, 193403 (2010).
- [26] H. Deng, H. Haug and Y. Yamamoto, *Rev. Mod. Phys.* **82**, 1489 (2010).
- [27] A. V. Paraskevov, Preprint arXiv:0902.3909 (2009).
- [28] P. Bak, C. Tang and K. Wiesenfeld, *Phys. Rev. A* **38**, 364 (1988).
- [29] L. V. Butov, *J. Phys.: Condens. Matter* **16**, R1577 (2004).
- [30] L. V. Butov *et al.*, Preprint arXiv:cond-mat/0308117 (2003).
- [31] P. Bak, *How nature works: The science of self-organized criticality* (Springer, New York, 1996).
- [32] H. L. Stormer *et al.*, *Phys. Rev. B* **41**, 1278 (1990).
- [33] M. P. Lilly *et al.*, *Phys. Rev. Lett.* **90**, 056806 (2003).
- [34] H. P. van der Meulen *et al.*, *Phys. Rev. B* **60**, 4897 (1999).
- [35] G. R. Facer *et al.*, *Phys. Rev. B* **59**, 4622 (1999).
- [36] A. V. Paraskevov and S. E. Savel'ev, *Phys. Rev. B* **82**, 119902(E) (2010).
- [37] U. Sivan, P.M. Solomon and H. Shtrikman, *Phys. Rev. Lett.* **68**, 1196 (1992).